A wind tunnel study of the effect of roadway configurations on the dispersion of traffic-related pollution

D. K. Heist[a,*], S. G. Perry[a] and L. A. Brixey[b]
[a]Atmospheric Modeling Division, National Exposure Research Laboratory, MD-81, U.S. Environmental Protection Agency, Research Triangle Park, NC 27711, USA
[b]Alion Science and Technology, P.O. Box 12313, Research Triangle Park, NC 27709, USA

*Corresponding author: David K. Heist, MD-81, U.S. Environmental Protection Agency, 109 T.W. Alexander Dr., Research Triangle Park, NC 27711, USA.
Email: heist.david@epa.gov. Phone: (919) 541-1199. Fax: (919) 685-3327.

Keywords: air quality, line source, dispersion modeling, wind tunnel, roadway configurations

Abstract

In this paper we examine the effect of different roadway configurations, including noise barriers and roadway elevation or depression relative to the surrounding terrain, on the dispersion of traffic-related pollutants for winds perpendicular to the roadway. A wind tunnel experiment modeling 12 different configurations was performed to study the flow fields and the concentration distributions resulting from emissions from a simulated six-lane highway. All of the configurations examined here reduced the downwind ground-level concentrations relative to that for a flat, unobstructed roadway; however, the degree to which the concentrations were reduced varied widely depending on the particular situation.

Ground-level concentration data from the cases considered in this research indicate that a constant entrainment velocity can be used over the region beginning downwind of any initial disturbance to the flow resulting from the roadway configuration (e.g., a recirculation region behind a noise barrier) and extending at least to the end of our measurements. For example, for the case of a single noise barrier on the downwind side of the road, this region extends from approximately four barrier heights downwind of the roadway to 40 barrier heights. It was also found that the virtual origin concept is useful in describing the initial

mixing created by the particular roadway configuration. To effectively model the influence of the roadway configuration on the dispersion, a combination of a virtual origin and an entrainment velocity may be effective. The magnitude of the virtual origin shift appears to depend on the particular roadway configuration, while the entrainment velocity appears to be a function of the friction velocity and the roadway geometry. These results suggest that road configuration must be taken into account in modeling near-road air quality.

1. Introduction

Studies have shown that long-term exposure to traffic-related pollutants is an important risk factor for a number of adverse health effects (Adar et al., 2007; Samet, 2007; Salam et al., 2008). In the U.S. there is increasing concern specifically for the many people that live, work, and attend school in close proximity to major roadways. Many applied dispersion models currently in use were developed for simplified roadway scenarios that do not include the complex geometries often found surrounding urban highways. Hosker et al. (2003) found that guidance for the application of such models in these situations has not been adequate, noting that problems can be anticipated in applying some dispersion models in areas with complex highway configurations and at urban intersections.

While a number of wind tunnel studies (e.g., Hayden et al., 2002; Kastner-Klein and Plate, 1999) have examined the effects of urban street canyons and intersections, there is a need to examine the influence of roadway configurations and nearby structures where urban buildings do not dominate the overall flow. Field studies (e.g., Zhu et al., 2002) near major roadways have shown an approximately exponential decrease in traffic-related pollutant concentration downwind of the road and a sensitivity to the presence of near-road structures such as noise barriers (Baldauf et al., 2008). Therefore, the wind tunnel study described here has been designed to consider these influences on the flow and dispersion of traffic-related

pollutants within a few hundred meters of the roadway. While the concentrations on the roadway itself are expected to be sensitive to the roadway configuration, this study is focused on the concentrations downwind of the road where people who live, work, and attend school may experience significant, long-term exposures.

Twelve roadway configurations were chosen for this study representing a range of typical configurations in use across the U.S. including noise barriers at various locations relative to the roadway, depressed roadways with vertical or sloping sidewalls, and an elevated roadway with sloping sidewalls down to the surrounding terrain. Results of detailed velocity and concentration measurements are presented for these cases.

One goal of this research is to provide data for use in developing algorithms for dispersion models that include the effects of roadway configurations. An initial analysis of the data suggests that concepts such as source offset and entrainment velocity can form the basis for improved algorithms. Our measurements suggest that offsetting the source location upwind a certain distance can account for the effect of a noise barrier on downwind, ground-level concentrations. The entrainment velocity (defined as the rate at which ambient air is entrained into the plume) has been used successfully in modeling hazardous pollutants where ground-level sources are common (Spicer and Havens, 1989; Witlox, 1994). Our data suggest that the ratio of this entrainment velocity to the friction velocity, although sometimes considered as a constant, is sensitive to roadway configuration and to the characteristics of the approach flow boundary layer. A recently proposed model for the dispersion of traffic-related pollutants from highways (Venkatram et al., 2007) can be written in terms of an entrainment velocity. This model is a good platform for including the effects of roadway configuration and approach flow characteristics on downwind dispersion. The data from this study is analyzed in light of these modeling concepts.

2. Experiment

The purpose of this experiment is to examine the effect of roadway configurations on the dispersion of traffic-related pollutants from the roadway up to distances of several hundred meters. Experiments were conducted in the U.S. EPA's Fluid Modeling Facility meteorological wind tunnel (Snyder, 1979). The test section is 370 cm wide, 210 cm high, and 1830 cm long. The air speed in the test section was fixed at 4.7 m s^{-1} at a height of 165 cm.

Twelve roadway configurations comprising various combinations of elevation changes relative to the surrounding terrain and noise barrier height and locations relative to the roadway were studied (Fig. 1). All cases were modeled as a six-lane, divided highway at a 1:150 scale. The basic length scale used to non-dimensionalize distances in the results presented in this paper is H, the height of most of the noise barriers used in this study and also the elevation and depth of the roadway relative to the surrounding terrain in cases not involving flat terrain. The full-scale equivalent value of H is 6 m. The origin of the coordinate system for the study is at the center of the roadway model on the tunnel floor, with x positive in the streamwise direction, y along the axis of the roadway, and z vertically upward.

Laser Doppler velocimetry (LDV) was used for all velocity measurements in this study. The LDV system used in these experiments was a two-component, single-probe system that employed the 488- and 514.5-nm lines from a Coherent Innova 70C argon-ion laser (Coherent, Inc., Santa Clara, CA). The beam splitting, frequency shifting, and coupling of laser light to fiber-optic cables were all performed with a TSI Colorburst multicolor beam separator (Model 9201, TSI Inc., St. Paul, MN). The LDV system was used in the real fringe mode with a frequency shift of 40 MHz to eliminate direction ambiguity in the velocity measurements. The use of a portable fiber-optic probe (TSI Model TR220 with a 110.0-cm focal distance lens) facilitated movement of the LDV measurement volume, an ellipsoid with

a diameter of ~65 μm and a length of ~0.1 cm. The LDV probe, measuring 2.5 cm in diameter and 18 cm in length, was mounted on the wind tunnel carriage for computer-controlled positioning.

The seeding material for the LDV was generated using a Rosco 1600 Fog Machine (Rosco USA, Stamford, CT) and introduced into the tunnel through a 2.5-cm hole in the wind tunnel floor located approximately 5.0 cm upwind of the central boundary layer generating spire. By injecting the particulate matter at this location, there was sufficient time and distance for the material to disperse across the width of the tunnel before reaching the model. At each location simultaneous measurements of the two components of velocity were acquired at a frequency of 20 Hz over a 120-s interval. Mean velocities and standard deviations were computed from these samples. At each location where velocity measurements were made, two separate measurements were performed in order to obtain all three components of velocity.

The boundary layer used in the majority of cases in this experiment was designed to simulate flow in an urban area. The boundary layer was created with three truncated Irwin spires (original height = 245 cm truncated at 210 cm to fit in the wind tunnel, base width = 45.5 cm, and lateral spacing [center to center] = 122 cm) at the inlet of the test section (Irwin, 1981). To condition and maintain the boundary layer, the floor of the test section downwind of the spires was covered with roughness blocks 7.6 cm high, 3.8 cm long in the streamwise direction, and 7.6 cm wide in a staggered pattern. These blocks were aligned in lateral rows with 7.6-cm (one block width) spacing. The rows were spaced by 15.2 cm in the alongwind direction with the blocks in subsequent rows offset laterally by one block width. Thus, the roughness blocks covered 12.5% of the floor area. The tunnel ceiling was adjusted along the length of the test section to compensate for blockage effects and allow for a non-accelerating freestream flow.

To examine the effect of boundary layer roughness on the results, two of the 12 configurations were repeated with a somewhat smoother boundary layer. This boundary layer was created with five Irwin spires (height = 148.3 cm, base width = 22.4 cm, and lateral spacing [center to center] = 74.1 cm) at the inlet of the test section followed by tab-type roughness elements (height = 3.8 cm, width = 7.6 cm, and spacing = 30.5 cm in both the lateral and longitudinal directions) similar to those used in Snyder (2001).

The standard logarithmic velocity profile was used to assess the roughness length (z_0), displacement height (d), and friction velocity (u_*):

$$\frac{U}{u_*} = \frac{1}{\kappa} \ln\left(\frac{z-d}{z_0}\right) \tag{1}$$

where κ, the von Karman constant, was taken to be 0.4. This equation was fit to the data (varying d and z_0) until the computed value of u_* matched the value found from the turbulent shear stress measurements. The fit was performed in the range from z = 15 to 40 cm, in the region of nearly constant turbulent shear stress. For the first boundary layer setup described, the best fit parameters were found to be z_0 = 0.52 cm, d = 5.4 cm, and u_* = 0.3 m s^{-1}. At a scale of 1:150, this corresponds to z_0 = 0.78 m and d = 8.1 m, characteristic of an urban surface form with a medium height and density of structures (Grimmond and Oke, 1999). The resulting boundary layer using the second setup described above had an equivalent full-scale roughness length scale of 0.27 m and a displacement height of 0 m, a roughness slightly less than that for the low height and density urban category of Grimmond and Oke (1999). Mean velocity profiles are shown in Fig. 2a along with the best fit described above for the two boundary layers used in this study. Fig. 2b shows the standard deviations of the velocity fluctuations normalized by u_* showing good agreement with those values observed in the atmosphere (σ_u/u_* = 2.5, σ_v/u_*= 1.9, σ_w/u_*= 1.3; Panofsky and Dutton, 1984).

To simulate the traffic along a six-lane highway, a roadway 280 cm long and 24 cm wide (420 m by 36 m, full scale) was installed in the wind tunnel with the roadway perpendicular to the wind direction. At the center of the roadway laterally, a source measuring 48 cm long and 24 cm wide (72 m by 36 m, full scale) was mounted. The source construction, illustrated in Fig. 3a, consists of three plates of aluminum: the bottom plate, with two holes to connect to the source gas; the middle plate, hollowed out to form the perimeter of the box; and the top plate, with six lines of small holes forming the emission lines. The assembled box, including gaskets between the plates, had an overall depth of approximately 3 cm. The emission lines, oriented parallel to the axis of the highway, each contained approximately 30 small holes (0.1 cm diameter) uniformly spaced with the holes in subsequent lines staggered to provide a near-continuous release along the length of the road source area. The uniformity of the concentration was measured at ground level at the downwind edge of the model roadway where measurements showed a coefficient of variation of 4.4%. To enhance the near-road turbulence, blocks measuring 0.6 by 0.6 by 1.2 cm were placed approximately 0.1 cm upwind of each release hole. This block pattern was continued the length of the road to maintain the lateral homogeneity of the roadway structure.

The tracer gas used in this study was high-purity ethane (C_2H_6; CP grade; minimum purity 99.5 mole percent), which with a molecular weight of 30 is only slightly heavier than air. In combination with the high turbulence level at the release point and a total release rate, Q, of only 1500 cc min^{-1}, this tracer may be regarded as neutrally buoyant.

All samples were drawn through Rosemount Model 400A hydrocarbon analyzers (flame ionization detectors). The output signals from the analyzers were digitized at the rate of 20 Hz (each unit) for 120 s and were processed on a personal computer.

After measuring the pattern of downwind concentration from the finite line segment, the infinite line source "results" can be constructed by superimposing the results from the finite line source, employing a lateral shift in the source location as follows:

$$C(x,z) = \sum_{i=-\infty}^{\infty} C_{fls}(x, y + iL_y, z), \tag{2}$$

where $C(x,z)$ is the predicted concentration downwind of an infinite line source and C_{fls} is the measured concentration based on a finite line source of width L_y. An example of this superpositioning is shown in Fig. 3b, where a lateral profile of the measured ground-level concentrations at $x = 30H$ is shown for the case where a noise barrier is installed upwind of the roadway. The measured ground-level concentrations are shown as filled diamonds. The open diamonds represent those measurements shifted laterally by multiples of the source width ($\pm 1L_y$ and $\pm 2L_y$). The solid line is the summation of the five profiles shown and demonstrates that there is a central portion which is uniform in the y direction, as if it were measured from an infinitely wide source.

The concentrations were normalized to give the non-dimensional concentration $\chi = CU_r/(Q/L_xL_y)$, where C is the concentration (a fraction by volume) with background concentration subtracted, U_r is the reference wind speed (equal to 2.46 m s^{-1}, measured at a full-scale equivalent height of 30 m), Q is the volumetric effluent rate (1500 cm^3 min^{-1} of ethane), L_x is the alongwind dimension of the roadway segment (24 cm, 36 m full scale), and L_y is the lateral length of the source segment (48 cm, 72 m full scale). Concentration measurements scaled in this way provide for easy comparisons with results from other (e.g., full-scale) situations with different wind speeds and emission rates when those results are non-dimensionalized in the same way. For a few selected locations, concentration measurements were repeated at a 50% higher reference wind speed, and normalized

concentration profiles at both wind speeds were in very good agreement, indicating the results were independent of Reynolds number.

3. Results and discussion

3.1 Impact of road configuration on the flow field

Ninety-one vertical velocity profiles were measured for nine different roadway configurations. Velocity profiles in three of the noise barrier cases were not measured (cases J, K, and L) because of the similarity of the geometry to cases that were measured (e.g., cases G and H). A subset of the results are shown in Fig. 4 focusing on the region between x/H = -10 and 10 where most of the variations among the cases occurs. In Fig. 4, the mean velocity vectors measured in the x-z plane at $y/H = 0$ are plotted and represent conditions averaged over 2 min.

For the flat terrain case (Fig. 4a), minor disturbances to the flow are seen over the source in an otherwise undisturbed flow. The elevated roadway (Fig. 4b) causes lifting of the streamlines and a small amount of recirculation in the lee of the roadway. The depressed roadway cases with vertical side walls show evidence of recirculating flow in the mean velocity vectors (Fig. 4c and 4d). Not surprisingly, the strength of the recirculation is enhanced in the deeper road cut (Fig. 4d). The depressed roadway with 30° sloping sides (Fig. 4e) creates no mean recirculation, although the histograms of longitudinal velocity (not shown) do indicate some intermittent negative velocities in the depressed region. The addition of noise barriers to the depressed roadway (Fig. 4f) creates substantial recirculation over the roadway and downwind of the roadway. The flat terrain cases with a single noise barrier (Figs. 4g and 4h) have a recirculation region that extends roughly $5H$ downwind of the barrier. Results for the case with a barrier on both sides of the roadway (Fig. 4i) show a recirculation between the barriers with a shortened (roughly $3H$) recirculation downwind of

the barrier. The turbulent kinetic energy calculated from the LDV measurements showed that the greatest increases in turbulent kinetic energy were caused by the velocity shear due to the presence of noise barriers.

3.2 Impact of road configuration on the concentration field

Contours of the concentration fields for the 12 cases were created from estimates of the infinite line source results made by the superposition method described above. These concentration contours are shown in Fig. 5. The elevated roadway concentration patterns look more like those from the flat terrain case than any other roadway configuration examined, especially at ground level. In these cases, the $\chi = 5$ contour extends the farthest downwind, reaching past $x = 30H$ (see Figs. 5a and 5b). For the other roadway configurations, this band reaches no farther downwind than $x = 25H$. The cases with noise barriers tend to lift the plume more than the other cases, with the $\chi = 5$ contour reaching $z = 2.5$ to $3H$ before descending again. In the cases without the barriers the maximum height of the $\chi = 5$ contour is roughly $z = 1.5H$ (with the exception of the elevated roadway case).

Fig. 6 shows vertical profiles of concentration at two downwind locations for five selected cases. Above ground level and closer to the source, there is a significant difference between the flat terrain (A) and elevated (B) cases, but this difference diminishes as the plume moves downwind. Not unexpectedly, in the elevated roadway case the plume peak concentration is significantly elevated above the surface. The other cases (E, F, and G) show lower concentrations by at least a factor of two, with the lowest concentrations seen for case F when the effect of a depressed roadway is combined with that of noise barriers.

To examine the effect of roadway geometry on pollutant dispersion, we begin by comparing the concentrations for four different cases by computing their ratios with the concentrations measured in the flat terrain case (χ_A) at the same locations. Fig. 7 shows these ratios for heights ranging from ground level to four times the barrier height, each as a

function of downwind distance. Enhanced vertical mixing resulting from the roadway configurations results in higher concentrations ($\chi/\chi_A > 1$) at heights above $1H$ and lower concentrations ($\chi/\chi_A < 1$) below $1H$ relative to the flat terrain case. These differences are most pronounced just downwind of the road, with ratios decreasing with downwind distance. Beyond $15H$ nearly all of the ratios are less than a factor of two. The largest departure from the flat case is the depressed roadway with noise barriers on both sides of the road, especially near ground level (Fig. 7c). The elevated roadway case (Fig. 7a) exhibits the least difference relative to the flat terrain case.

To investigate the effect of noise barrier placement, Fig. 8 shows the concentration ratios for several different barrier cases to the case of the barrier at $x/H = -3$ (Case G). Note that the vertical scale in Fig. 8 spans only two orders of magnitude, in contrast to the three spanned in Fig. 7. The effect of noise barrier placement appears to be much smaller than the effects seen in Fig. 7d where case G is compared to the flat terrain case. At downwind distances of $10H$ and beyond, the differences in concentration ratios are less than 20% relative to the case with the noise barrier located at the upwind edge of the roadway. Between the edge of the roadway ($3H$) and $10H$ the largest difference seen in the cases examined here is approximately a factor of two.

Fig. 9a shows the behavior of ground-level concentration as a function of downwind distance for four different cases including flat terrain, noise barriers and depressed roadways. Fig. 9b shows a plot of the inverse ground-level concentration as a function of x/H for the same cases. In Fig. 9b, the trend of the data for each case appear to be offset from one another, suggesting that a simple upwind shift in the flat terrain results may be used to describe the measured concentrations in the other cases. The solid line in Fig. 9b is the best-fit straight line to the flat terrain data. Using the concept of a virtual origin, this line can be shifted upwind to examine how it compares to the data for the other cases. Fig. 9b shows

examples of this for shifts of $6H$ and $11H$ bracketing the range of results. The magnitude of the virtual origin shift appears to depend on the particular roadway configuration in question, with the largest shift required when multiple effects are present in one configuration (e.g., depressed roadway with noise barriers on both sides of the road). Fig. 9a shows the straight lines from Fig. 9b plotted as χ_s versus downwind distance.

3.3. Entrainment velocity

The plots in Fig. 8 and 9 suggest that downstream of a certain point (perhaps 7 to $10H$) some cases behave similarly enough that their concentration distributions may be parameterized similarly within a dispersion model. One parameter that has been found useful in modeling ground-level releases, and has been used particularly in hazardous release models, is the vertical entrainment velocity, w_e (Spicer and Havens, 1989; Witlox, 1994).

Briggs et al. (2001) have defined w_e as the "effective rate at which ambient fluid is mixed vertically into the plume to dilute its concentration." From this definition, an expression for w_e can be developed that relies on easily measured quantities available from the concentration measurements in this study, namely, the ground-level concentration (C_s) and the emission rate per unit length of roadway (Q/L_y):

$$w_e = \left(\frac{Q}{L_y}\right)\frac{d\left(\frac{1}{C_s}\right)}{dx} \tag{3}$$

It should be noted that the use of the entrainment velocity to characterize the growth of the plume is focused in this discussion on the ground-level concentrations, but can also be related to elevated concentrations with the use of assumptions about the shape of the vertical distributions since $w_e \propto \frac{d\sigma_z}{dt}$ (Britter et al., 2003). In Fig. 9b, the inverse ground-level concentrations as a function of x/H do appear to follow a straight line (as suggested by

equation 3) beyond approximately $x = 7H$, implying that the entrainment velocity is constant over the range $7H$ to at least $40H$.

The experiments described above were all performed using a fairly rough boundary layer characteristic of a medium-density urban region. To begin to examine the sensitivity of these results to the roughness length of the boundary layer, we constructed a boundary layer that can be characterized as slightly less dense than the "low height and density" category of Grimmond and Oke (1999) with an equivalent full-scale roughness length scale of 0.27 m and a displacement height of 0 m. This contrasts with the original boundary layer with $z_0 =$ 0.78 m and $d = 8.1$ m.

With this smoother approach flow, concentration measurements for the flat terrain case (Case A) and the case with a single barrier at $x/H = 3$ (Case H) were repeated. The ground-level concentration measurements are shown in Fig. 10, along with the inverse of the concentrations as a function of downwind distance (scaled differently; see below). By dividing both sides of equation 3 by u_* the ratio w_e/u_* is found to equal $d/dx(Q/(C_s u_* L_y))$. In Fig 10b, therefore, the straight-line fit to a plot of $Q/(C_s u_* L_y)$ versus x has a slope equal to w_e/u_*. The results from the rougher boundary layer are included in this figure for comparison. As seen in Fig. 10a, the two flat terrain cases start with similar concentrations at the edge of the roadway (differing by less than 7%), but the concentrations in the rougher boundary layer drop off more quickly with downwind distance. When a noise barrier is introduced at the downwind edge of the road (Case H), the concentrations at the edge of the road start at quite different levels (differing by more than 30%) and fall with downwind distance. The concentration decrease with downwind distance is still enhanced with the rougher boundary layer, but to a lesser extent than in the flat terrain case (we will return to this point below).

Britter et al. (2003) reviewed several theoretical and experimental estimates for the ratio w_e/u_* and noted that in many studies this ratio depends on the exponent of the velocity

profile power-law (p) or the profile exponent of the vertical concentration distribution. However, Briggs et al. (2001) and Britter et al. (2003) found w_e/u_* to be a constant (0.65 ± 0.05) for the diffusion of a ground-level line source in a rough wall boundary layer. An alternative derivation mentioned by Briggs et al. (2001), however, did yield w_e/u_* equal to $0.53(1+p)$. This implies a larger entrainment velocity for rougher boundary layers. The cases reported here suggest that the rate of entrainment of ambient air into the plume may be affected by the boundary layer roughness length scale. A recently proposed model for the dispersion of traffic-related pollutants from highways that can account for a variation of entrainment velocity with boundary layer roughness (Venkatram et al., 2007) takes the following form for near-neutral conditions:

$$\frac{C(x,z)}{Q/L_y} = \frac{A}{a\sigma_w x + b}\exp\left[-\left(\frac{Bz}{\bar{z}}\right)^s\right] \tag{4}$$

Here, s is the shape factor for the vertical concentration profile, $\bar{z}$ is the mean plume height, σ_w is the standard deviation of the vertical velocity fluctuations, A and B are functions of s only, a is a function of s and p, and b is a function of p, s, z_r, U_r (a reference velocity at height z_r), wind angle, and h_o (the release height). In the derivation of this equation, they used $u_* = \sigma_w/\alpha$, where α equals 1.25. For ground-level concentrations, this reduces to

$$\frac{Q/L_y}{u_* C_s} = \left(\frac{a\alpha}{A}\right)x + \left(\frac{b}{Au_*}\right). \tag{5}$$

Using the definition above for entrainment velocity, we find

$$\frac{w_e}{u_*} = \frac{a\alpha}{A} = fn(p,s). \tag{6}$$

Therefore, according to the Venkatram et al. (2007) formulation, one would expect the entrainment velocity to depend on the shape of the vertical velocity and concentration profiles in addition to the dependence on u_*. Also, the upwind shift in the concentration

profiles found above for several cases relative to the flat terrain case (described as a virtual origin) can be thought of as being contained in the parameter $b/(Au_*)$, a function of several parameters including profile shapes and release height.

A plot of $(Q/L_y)/(u_*C_s)$ versus downwind distance, x, beyond the immediate effects of the roadway obstacles produces a straight line whose slope is the ratio w_e/u_*. Fig. 10b shows such a plot for four different cases: flat terrain and a noise barrier on the downwind side of the roadway in boundary layers representative of both a low-density and medium-density urban area. The ratio w_e/u_* increases from 0.60 for the low-density urban area flat terrain case to 1.01 for the medium-density noise barrier case. In comparison, Britter et al. (2003) concluded from an analysis of three separate wind tunnel experiments that a value of 0.65 ± 0.05 characterized the parameter w_e/u_* for ground-level, neutrally buoyant line source releases in a neutrally stratified boundary layer without the presence of any nearby structures. Therefore, it appears that modeling the downwind concentrations of traffic-related pollutants from highways may require algorithms for both the entrainment velocity and the virtual origin as functions of boundary layer parameters and roadway geometry. The formulation of equation 4 using σ_w instead of u_* may prove to be more useful in these near-ground-level plumes that are spread by turbulence generated by near-road structures that has not come to equilibrium with the boundary layer turbulence characterized by u_*.

5. Summary

This paper has focused on the effect of 12 different roadway configurations, including noise barriers and roadway elevation or depression relative to the surrounding terrain, on the dispersion of traffic-related pollutants. A wind tunnel study was performed to examine the flow fields and the concentration distributions resulting from emissions from a six-lane highway for these 12 configurations.

Of the configurations studied here, each one had the effect of reducing the ground-level pollutant concentrations downwind of the roadway as compared to the flat terrain case with no barriers. The smallest reduction in ground-level concentration occurred for the elevated roadway, and the largest reduction was for the case that combined a depressed roadway with a noise barrier on both sides of the roadway. Ground-level concentrations were found to be substantially reduced by the addition of a barrier to the flat terrain case, but much smaller differences were observed as the location of the barrier was changed.

One parameter that has been found useful in modeling ground-level releases and has been used particularly in hazardous release models is the vertical entrainment velocity, w_e. For the cases considered in this paper, ground-level concentration data indicate that for each configuration a constant entrainment velocity applies over the region beginning $4H$ downwind of the edge of the roadway and extending at least to the end of our measurements at $37H$ downwind of the roadway.

To model the concentrations downwind of various roadway configurations, a combination of a virtual origin shift and an entrainment velocity that is a function of the friction velocity as well as roadway geometry may be effective. The magnitude of the virtual origin shift appears to depend on the particular roadway configuration in question. The model described in Venkatram et al. (2007) would serve as a good platform upon which to build algorithms incorporating the modeling concepts discussed in this paper.

The experiments reported here focused on winds perpendicular to the roadway for two boundary layer conditions. A fuller exploration of the effects of the boundary layer parameters and the wind direction will be needed to determine if the modeling concepts explored can be expanded to incorporate them.

Acknowledgements

The authors would like to thank Tom Pierce, Vlad Isakov, Alan Vette, Roger Thompson, John Rose, and George Bowker for helpful discussions, valuable comments, and assistance in model building. The authors are grateful to Rich Baldauf, Dan Costa, and David Kryak for collaboration and programmatic support.

Disclaimer

The United States Environmental Protection Agency through its Office of Research and Development funded and managed the research described here under contract EP-D-05-065 to Alion Science and Technology. It has been subjected to Agency review and approved for publication. Mention of trade names or commercial products does not constitute endorsement or recommendation for use.

References

Adar, S.D., Kaufman, J.D. 2007. Cardiovascular disease and air pollutants: evaluating and improving epidemiological data implicating traffic exposure. Inhalation Toxicology 19(1), 135-149.

Baldauf, R., Thoma, E., Khlystov, A., Isakov, V., Bowker, G., Long, T., Snow, R., 2008. Impacts of noise barriers on near-road air quality. Atmospheric Environment 42, 7502-7507.

Briggs, G.A., Britter, R.E., Hanna, S.G., Havens, J.A., Robins, A.G., Snyder, W.H., 2001. Dense gas vertical diffusion over rough surfaces: results of wind-tunnel studies. Atmospheric Environment 35, 2265-2284.

Britter, R.E., Hanna, S.G., Briggs, G.A., Robins, A.G., 2003. Short-range vertical dispersion from a ground level source in a turbulent boundary layer. Atmospheric Environment 37, 3885-3894.

Grimmond, C.S.B., Oke, T.R., 1999. Aerodynamic properties of urban areas derived from analysis of surface form. Journal of Applied Meteorology 38, 1262-1292.

Hayden, R.E., Kirk, W.D., Succi, G.P., Witherow, T., Bouderba, I., 2002. Modifications of Highway Air Pollution Models for Complex Geometries – Volume II: Wind Tunnel Test Program. U.S. Department of Transportation, Federal Highway Administration Report, FHWA-RD-02-037.

Hosker, R.P, Jr., Rao, K.S., Gunter, R.L., Nappo, C.J., Meyers, T.P., 2003. Issues affecting dispersion near highways: light winds, intra-urban dispersion, vehicle wakes, and the ROADWAY-2 dispersion model. U.S. Department of Commerce, NOAA Technical Memorandum OAR ARL-247.

Irwin, H.P.A.H., 1981. The design of spires for wind simulation. Journal of Wind Engineering and Industrial Aerodynamics 7, 361-366.

Kastner-Klein, P., Plate, E.J., 1999. Wind-tunnel study of concentration fields in street canyons. Atmospheric Environment 33, 3973-3979.

Panofsky, H.A., Dutton, J.A., 1984. Atmospheric Turbulence. Wiley, New York, 397pp.

Salam, M.T., Islam, T., Gilliland, F.D., 2008. Recent evidence for adverse effects of residential proximity to traffic sources on asthma. Current Opinion in Pulmonary Medicine 14(1), 3-8.

Samet, J.M., 2007. Traffic, air pollution, and health. Inhalation Toxicology 19(12), 1021-1027.

Snyder, W.H., 1979. The EPA Meteorological Wind Tunnel: Its Design, Construction, and Operating Characteristics, Report No. EPA-600/4-79-051, U. S. Environmental Protection Agency, Research Triangle Park, NC.

Snyder, W.H., 2001. Wind-tunnel study of entrainment in two-dimensional dense gas plumes at the EPA's fluid modeling facility. Atmospheric Environment 35, 2285-2304.

Spicer, T.O., Havens, J.A., 1989. User's guide for the DEGADIS 2.1 dense gas dispersion model. EPA-450/4-89-019, U.S. EPA, Research Triangle Park, NC 27711 USA.

Venkatram, A., Isakov, V., Thoma, E., Baldauf, R., 2007. Analysis of air quality data near roadways using a dispersion model. Atmospheric Environment 41, 9481-9494.

Witlox, H.W.M., 1994. The HEGADAS model for ground-level heavy-gas dispersion, I. Steady-state model. Atmospheric Environment 28, 2917-2932.

Zhu , Y., Hinds, W.C., Kim, S., Sioutas, C., 2002.Concentration and size distribution of ultrafine particles near a major highway. Journal of the Air & Waste Management Association 52, 1032-1042.

Figure Captions

Fig. 1. Elevation view showing cross sections through the various roadway configurations studied (cases A through L corresponding to figure lettering). Flow is from left to right. Dashed line in b) through f) represents at-grade elevation.

Fig. 2. Vertical profiles of a) measured mean horizontal velocity with log-law fits and b) rms velocities normalized by friction velocity (squares – σ_u/u_*, diamonds – σ_v/u_*, triangles – σ_w/u_*). Solid symbols – $z_0 = 0.78$ m, open symbols – $z_0 = 0.27$ m.

Fig. 3. Source layout. a) Geometry. 1 mm diameter emission holes arranged in six lines of approximately 30 holes each form source. Black squares indicate position of roughness elements upwind of each emission hole. Dimensions are full-scale meters. b) Superposition of concentration measurements from a finite line-segment source to create effect of an infinite line source. Results are measured at $x = 30H$ for case of an upwind noise barrier. Filled diamonds are measured results; open diamonds represent measured results shifted laterally by multiples of source width; solid line is summation of all five profiles; boxes on y/H-axis represent lateral positions of the five line-segment sources.

Fig. 4. Average velocity vectors measured with laser Doppler velocimetry for cases A through I (Figs. 4a through 4i, respectively). Reference vector at top shows magnitude of velocity at a height of 30 m ($5H$).

Fig. 5. Concentration contours for an infinite line source for cases A through L (Figs. 5a through 5l, respectively). Flow is from left to right.

Fig. 6. Vertical concentration profiles at a) $x/H \approx 5$ and b) $x/H = 10$. (A = flat terrain; B = elevated roadway, sloped wall; E = depressed roadway, sloped walls; F = depressed roadway, sloped wall, and noise barriers; G = noise barrier at $x/H = -3$.)

Fig. 7. Concentration ratios relative to flat terrain case for a) Case B - elevated roadway with 30° sloped wall. b) Case E - depressed roadway with 30° sloped walls. c) Case F - depressed roadway with 30° sloped wall and noise barriers at $x/H = \pm 4.7$. d) Case G - noise barrier at $x/H = -3$.

Fig. 8. Concentration ratios relative to case with noise barrier directly upwind of roadway ($x/H = -3$) for a) Case H - noise barrier at $x/H = 3$. b) Case I - noise barriers at $x/H = \pm 3$. c) Case K - noise barrier at $x/H = -4$. d) Case L - noise barrier at $x/H = -5$.

Fig. 9. a) Ground-level concentration as a function of downwind distance. b) Inverse ground-level concentration as a function of downwind distance. Solid line is a straight line fit to flat terrain data. Other lines show the effect of shifting source location for flat case a distance of $6H$ (dashed) and $11H$ (dotted) upwind. (A = flat terrain; E = depressed roadway, sloped walls; F = depressed roadway, sloped wall, and noise barriers; G = noise barrier at $x/H = -3$.)

Fig. 10. a) Ground-level concentration versus downwind distance for two boundary layer wind profiles with different roughness lengths and for two different roadway configurations (Cases A and H). b) Inverse ground-level concentration for the same cases, scaled to yield w_e/u_* as slope of best-fit line (axes units are full-scale meters). (A = flat terrain; H = noise barrier at $x/H = 3$.)

Figure 01

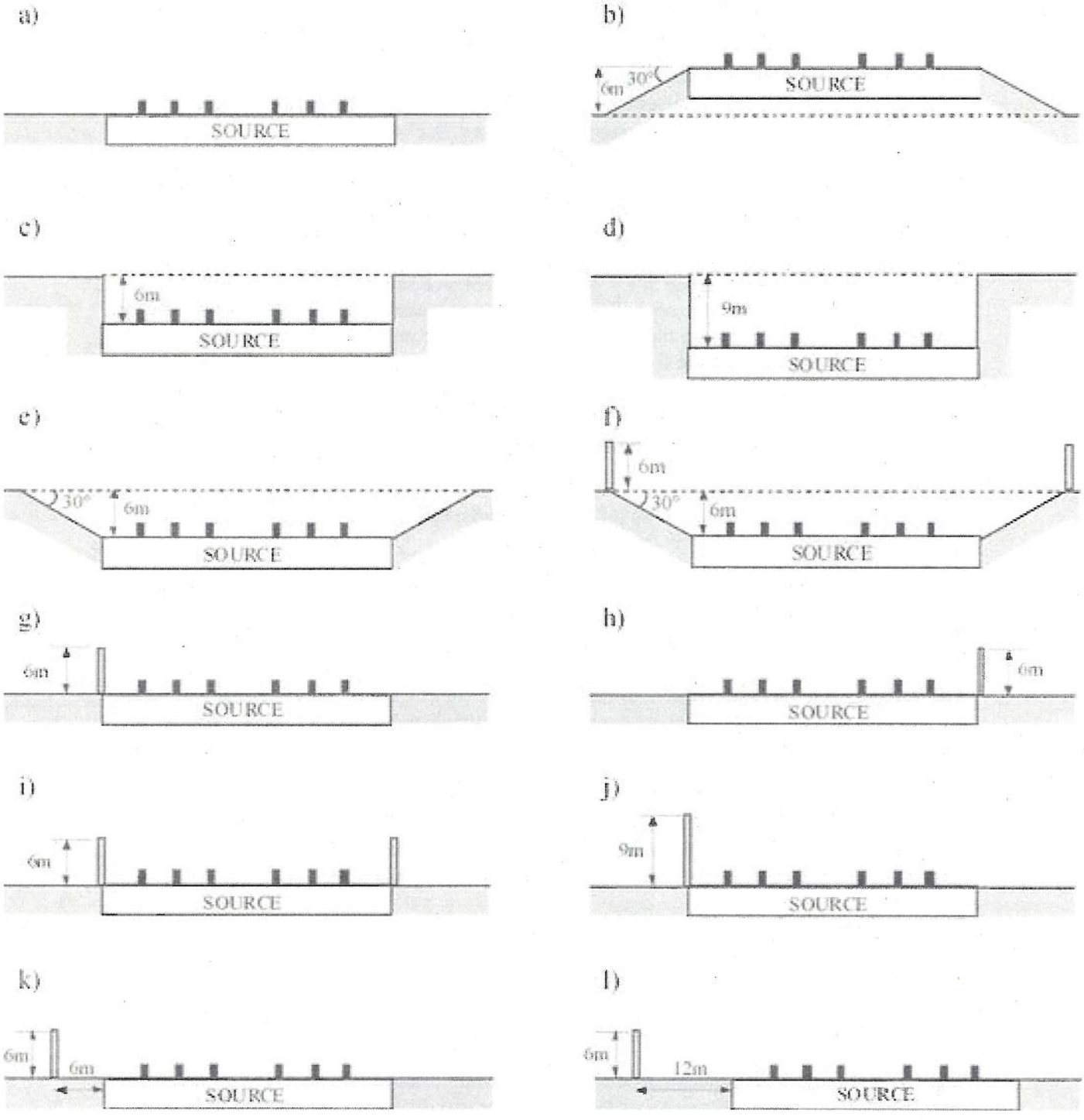
a)
SOURCE
b)
6m
30°
SOURCE
c)
6m
SOURCE
d)
9m
SOURCE
e)
30°
6m
SOURCE
f)
6m
30°
6m
SOURCE
g)
6m
SOURCE
h)
6m
SOURCE
i)
6m
SOURCE
j)
9m
SOURCE
k)
6m
6m
SOURCE
l)
6m
12m
SOURCE

Figure 02

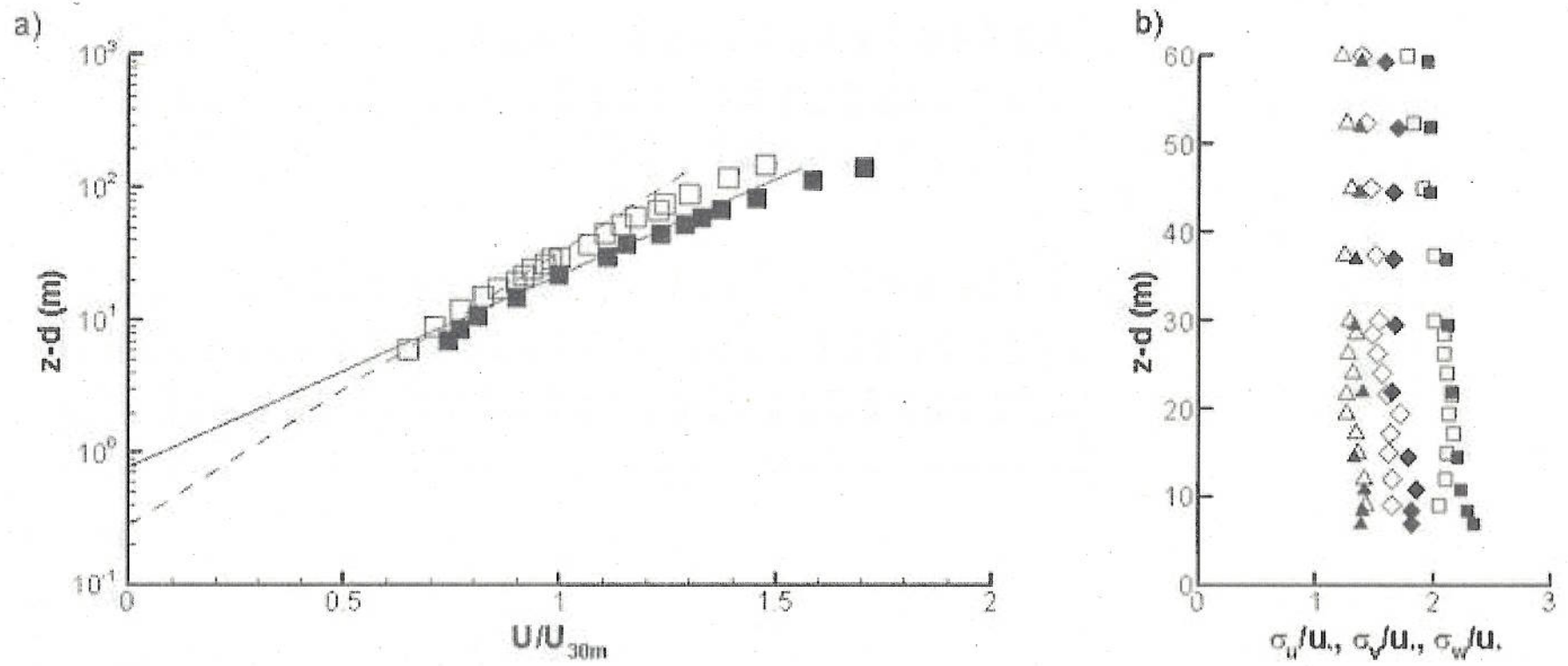

Figure 03a

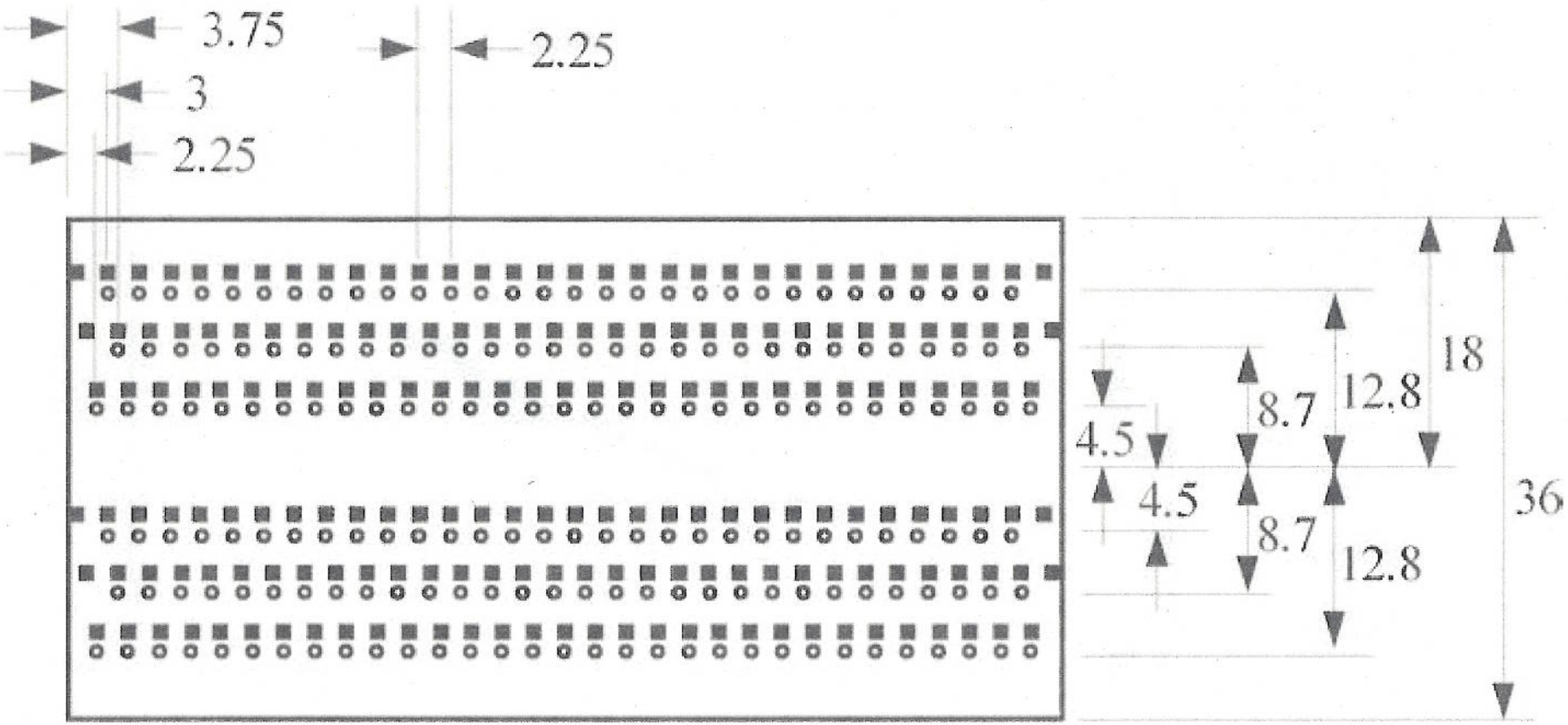

Figure 03b

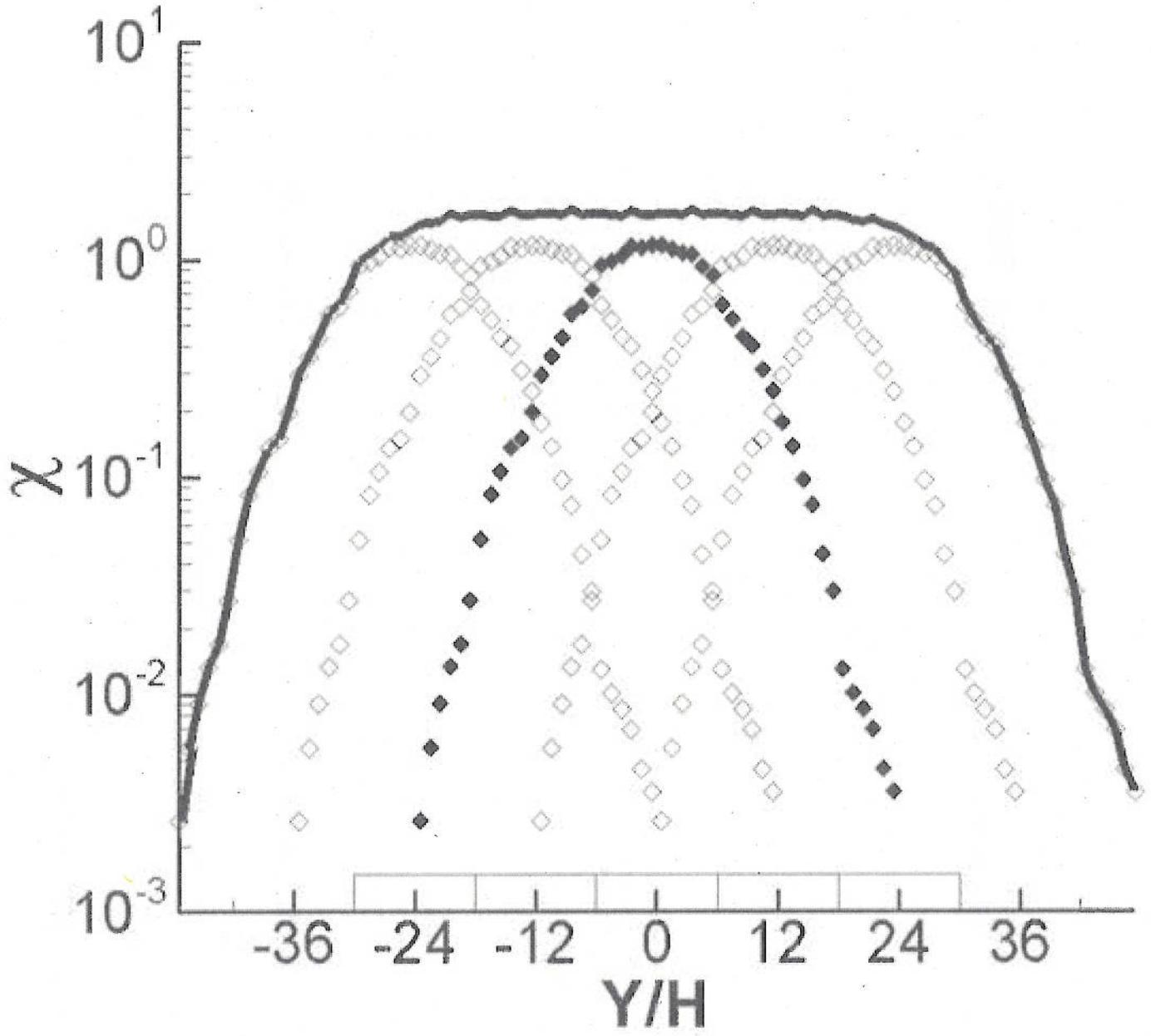

Figure 04

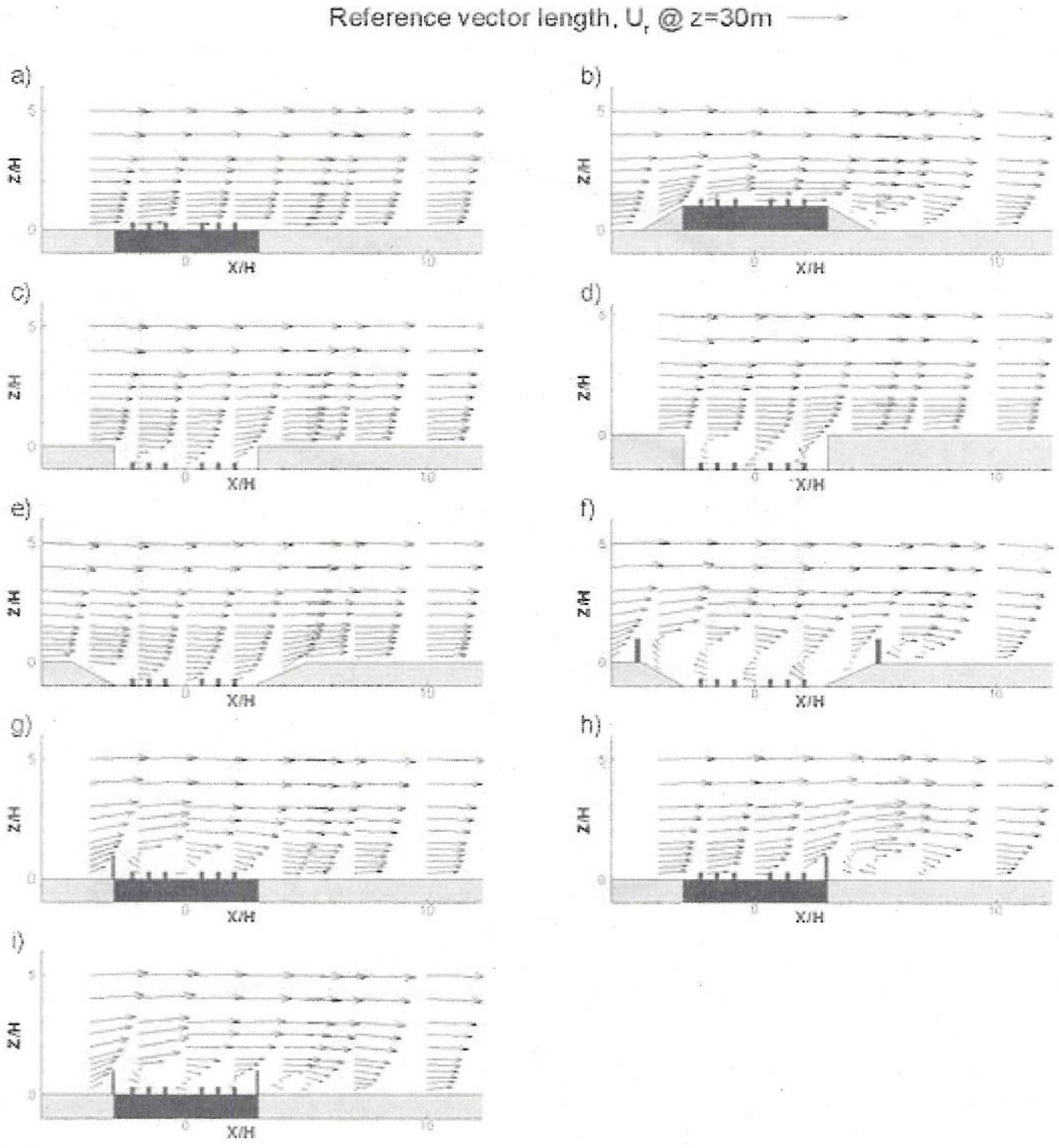

Figure 05

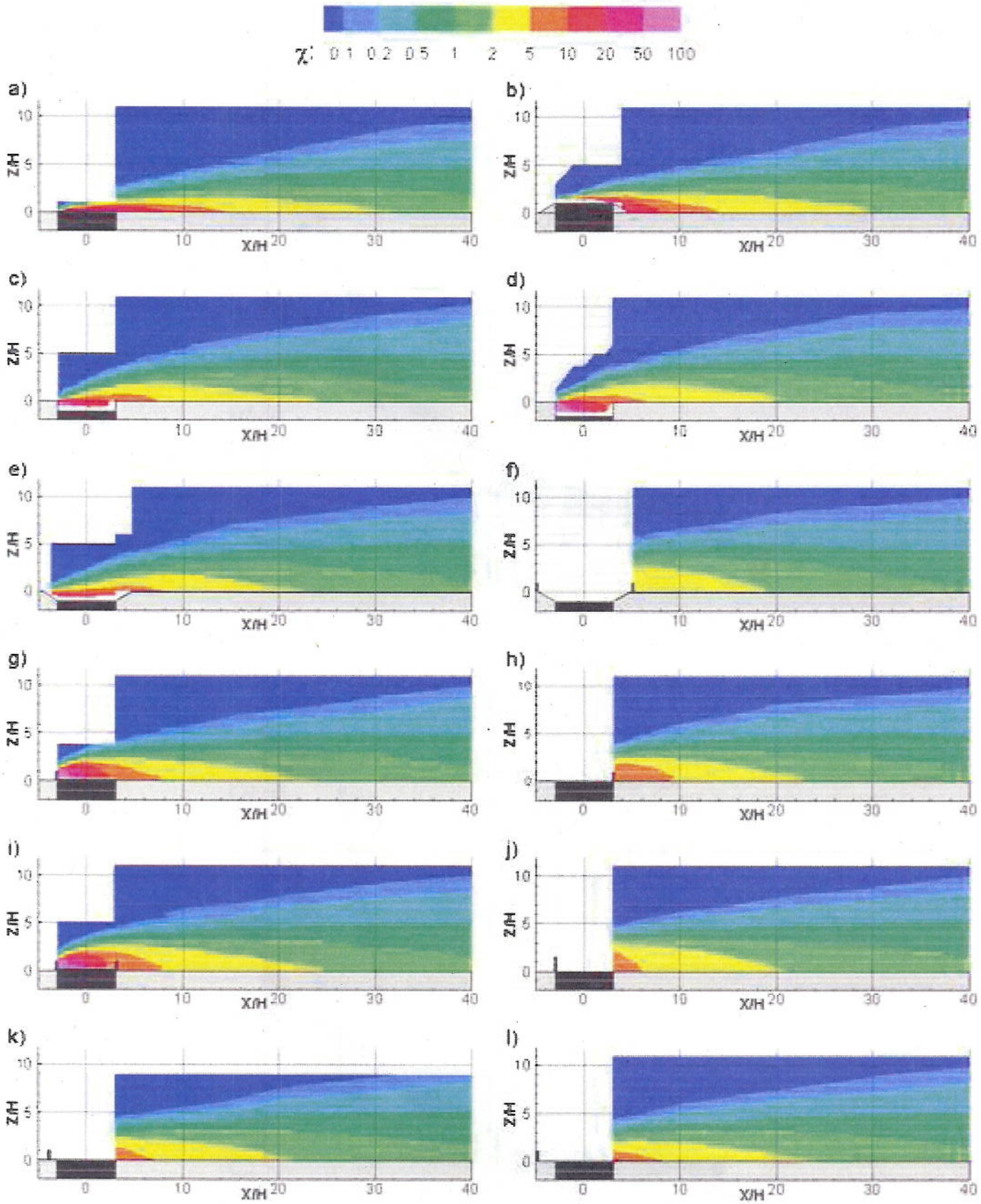

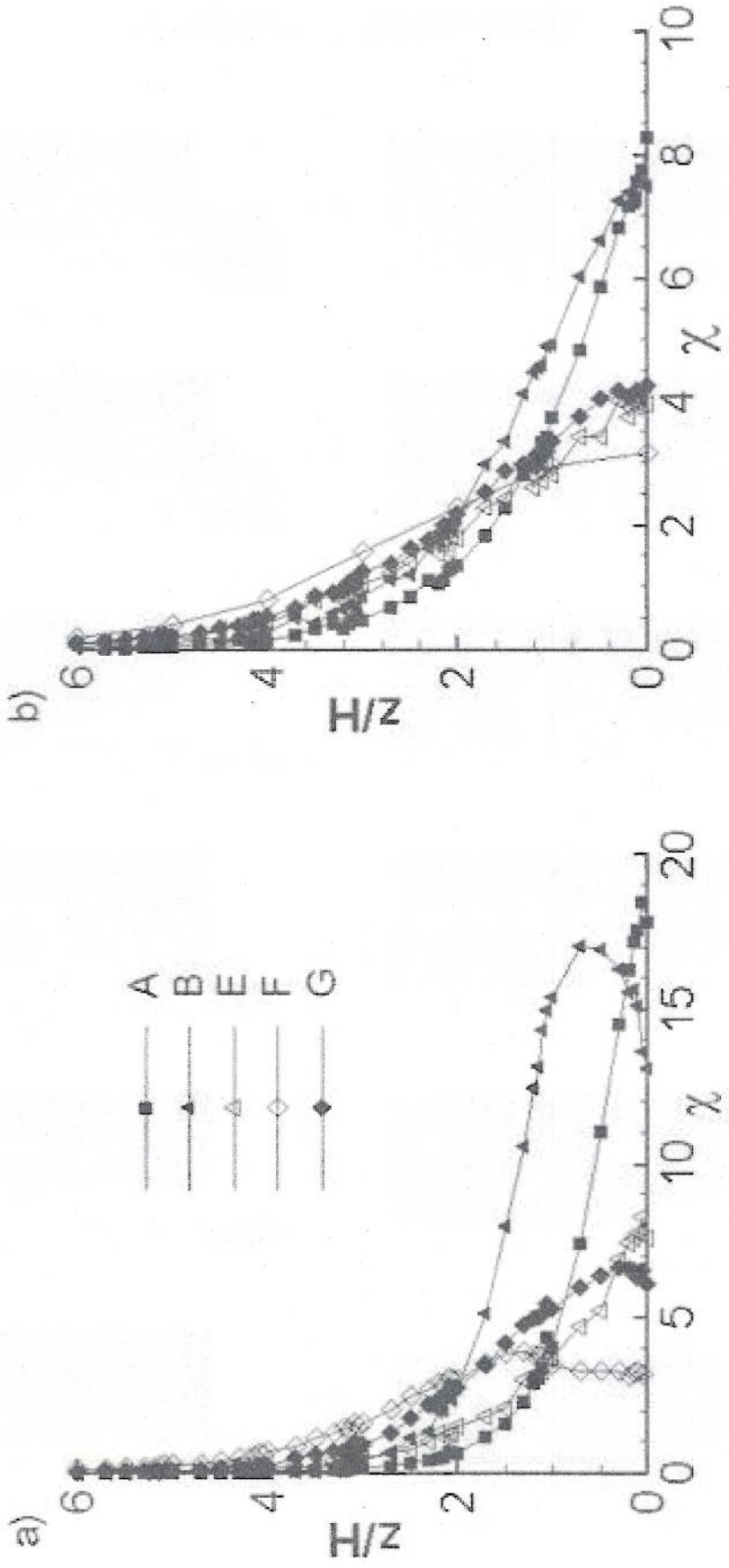

Figure 06

Figure 07

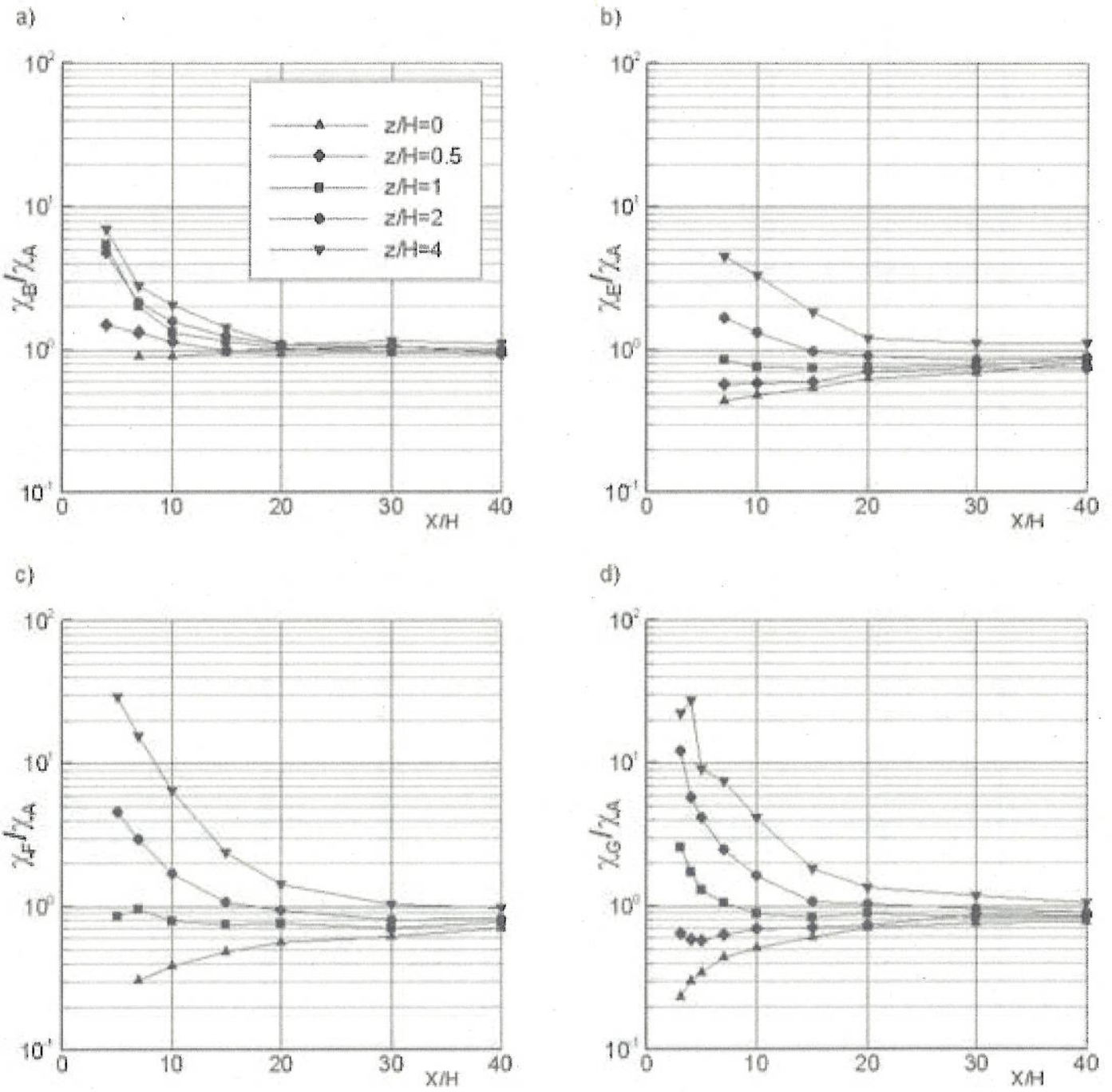
a)
b)
c)
d)
z/H=0
z/H=0.5
z/H=1
z/H=2
z/H=4
X/H
χ_B/χ_A
χ_E/χ_A
χ_F/χ_A
χ_G/χ_A

Figure 08

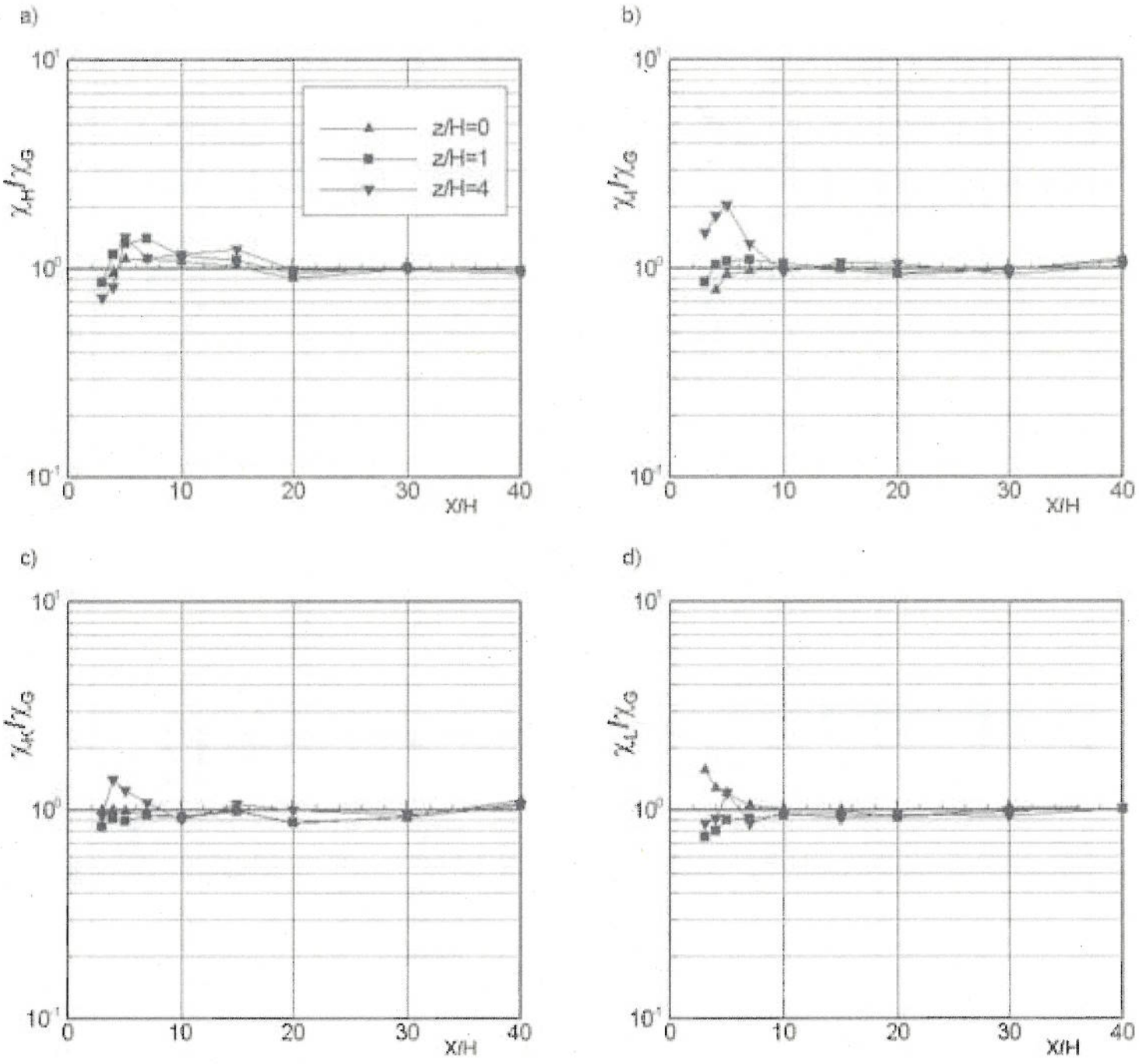

Figure 09

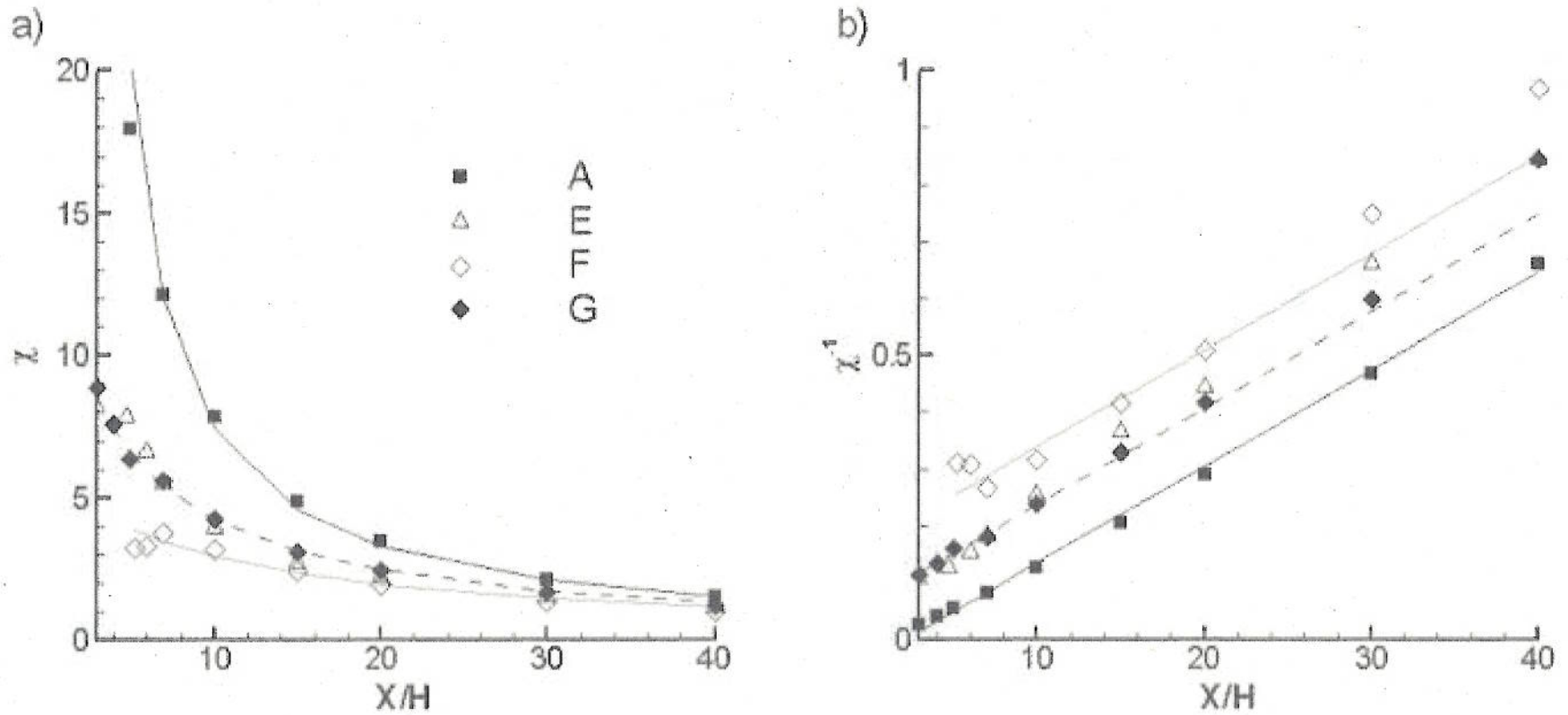

Figure 10

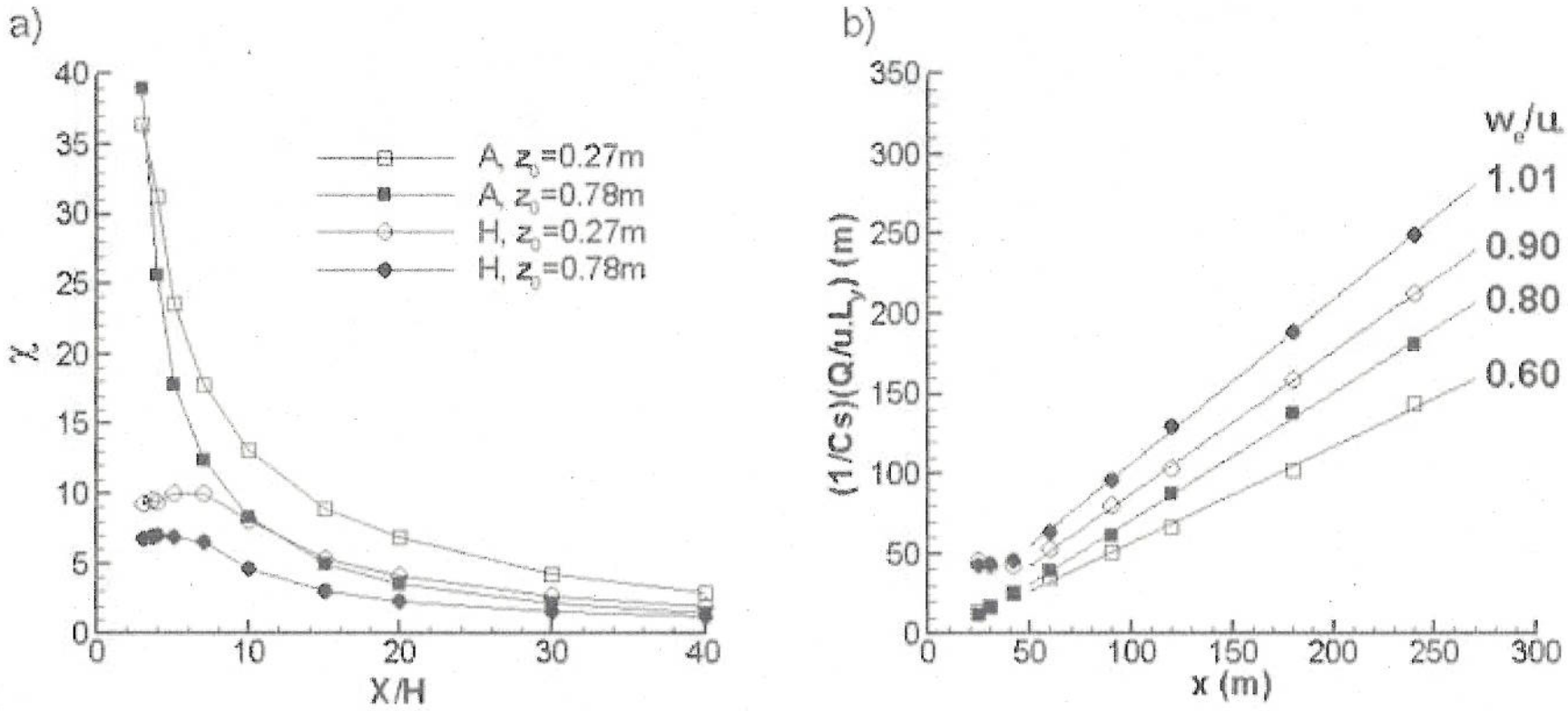
a)
χ
X/H
A, z0=0.27m
A, z0=0.78m
H, z0=0.27m
H, z0=0.78m
b)
(1/Cs)(Q/u.Ly) (m)
x (m)
we/u.
1.01
0.90
0.80
0.60